SACLANTCEN REPORT
serial no: SR-279

SACLANT UNDERSEA RESEARCH CENTRE REPORT

DETECTION OF BURIED OBJECTS IN THE SEABED - A SIMPLE MODEL STUDY

J.M. Hovem

October 1998

SACLANT Undersea Research Centre
Viale San Bartolomeo 400
19138 San Bartolomeo (SP), Italy

tel: +39-0187-540.111
fax: +39-0187-524.600

e-mail: library@saclantc.nato.int

NORTH ATLANTIC TREATY ORGANIZATION

SACLANTCEN SR-279

Detection of buried objects in the seabed
A simple model study

Jens M. Hovem

The content of this document pertains to work performed under Project 031-1 of the SACLANTCEN Programme of Work. The document has been approved for release by The Director, SACLANTCEN.

Jan L. Spoelstra
Director

intentionally blank page

Detection of buried objects in the seabed - a simple model study

Jens M. Hovem

Executive Summary:

The ability to model scattering from mines is important as it leads to an understanding of the frequency, temporal, and spatial features of the scattered pressure field, which may be exploited for detection and classification purposes. As mines are often buried, it is also very important to be able to model the effects of the sediment and the seabed interface on the scattering characteristics of the mine.

There is still much research to be done in improving the computational efficiency and the general applicability of models. There are also numerous techniques or approximations which should be investigated. Modelling yields important insights and information for the optimization of sonar detection and classification performance.

intentionally blank page

Detection of buried objects in the seabed - a simple model study

Jens M. Hovem

Abstract: The problem of detecting an object buried in the seabed is studied by means of a simple model. In this model, the object is a rigid sphere buried in a bottom modelled as a fluid half space. The scattered field is determined for all angles, including grazing angles lower than the critical angle. The analysis shows that the scattered field is considerably changed in amplitude and angular distribution, when the incoming wave is an inhomogeneous wave. There is relatively strong scattering in a broad angle interval, near the vertical direction. The detectability of a buried target is determined by the echo-to-reverberation level. This issue is discussed using a simple bottom reverberation model based on the small-roughness perturbation approximation. Signal-to-reverberation ratios are computed for different bottom types and for angles lower and higher than critical angle, for monostatic and bistatic detection situations.

Keywords:

Contents

1
Introduction

The purpose of this report is to study the echo formation process for the detection of an object buried in the sea floor and to estimate the signal to reverberation level in a detection situation. In view of recent interest, particular emphasis is given to situations where the target is insonified at very low grazing angles and both monostatic and bistatic situations are considered.

Scattering of buried objects is extensively treated in the literature [1], [2], [3]. Theoretical studies of realistic targets and environments requires numerical solutions. The danger with numerical solutions, is that sometimes, the physical aspects are hidden, with the consequence that it might be difficult to draw conclusions beyond the particular case. This report considers a very simple model, neglecting many potentially important mechanisms. The justification for studying a simple model, is to focus on some of the more important factors that are relevant to the more realistic and complicated situations.

The main part of this report considers scattering from a rigid sphere buried in the bottom. The incoming wave in the water is assumed to be a plane wave, which after refraction, is incident on the target. The water-bottom interface is plane and the bottom is modelled as an homogeneous fluid half-space, with a plane interface. For incident grazing angles above the critical angle, this is a simple problem. For incidence at grazing angles lower than critical, the incident wave on the target is an inhomogeneous wave. This case is treated in the same way as the homogeneous case, while exercising care to correctly include the evanescent scattering contributions which give the backscattering in the water, at grazing angles lower than the critical angle.

The second part of this study considers the bottom reverberation from a rough bottom. Bottom reverberation is determined by applying the simple scattering model for a rough surface, normally referred to as the Rayleigh - Rice approximation, assumed to be valid for high frequencies and relatively small roughness.

2

Scattering of a buried target

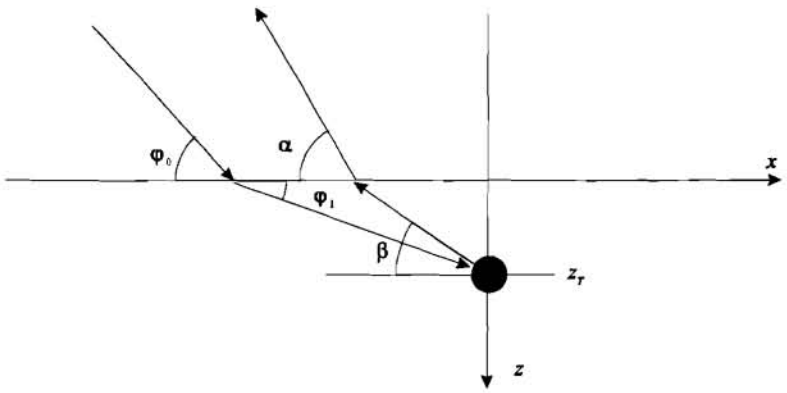

Figure 1 *Geometry of scattering of a buried object.*

In the geometry shown in Fig. 1, the water has density ρ_0, velocity c_0 and the bottom is a fluid with density ρ_1, sound velocity c_1. There is an incoming wave in the water with grazing angle,

$$\phi_0 = \hat{\phi}_0 \exp(ik_0 x \cos\varphi_0)\exp(ik_0 z \sin\varphi_0) \tag{1}$$

This wave is refracted at the interface and multiplied by the water-bottom transmission coefficient and propagating in the bottom as

$$\phi_1 = \hat{\phi}_1 \exp(ik_1 x \cos\varphi_1)\exp(ik_1 z \sin\varphi_1), \tag{2}$$

with $\hat{\phi}_1 = T_{01}\hat{\phi}_0$ and with the (pressure) transmission coefficient for the interface,

$$T_{01} = \frac{2\rho_1 c_1 \sin\varphi_0}{\rho_1 c_1 \sin\varphi_0 + \rho_0 c_0 \sin\varphi_1}. \tag{3}$$

Snell's law gives the relation between the angles,

$$\varphi_1 = \arccos\left(\frac{c_1}{c_0}\cos\varphi_0\right). \tag{4}$$

When the refracted wave strikes the target there is a scattered wave,

$$\phi_s = \hat{\phi}_1 S_1(\beta,\varphi_1)\exp(-ik_1 x\sin\beta)\exp(-ik_1 z\cos\beta). \tag{5}$$

Part of the scattered field of the target, $S_1(\beta,\varphi_1)$, is transmitted back through the bottom/water interface into the water. The intensity in the water, I_0, is the product of the transmitted pressure and the vertical component of the particle displacement,

$$I_0(\alpha) = \left|\hat{\phi}_1 S(\beta,\varphi) T_{10}\exp(ik_1 z_T\sin\beta)\right|^2 \frac{c_1\sin\alpha}{c_0\sin\beta}, \tag{6}$$

where the pressure transmission coefficient going from the bottom to the water is

$$T_{10} = \frac{2\rho_0 c_0\sin\beta}{\rho_0 c_0\sin\beta + \rho_1 c_1\sin\alpha}, \tag{7}$$

and the angles α and β are the scattering angles with respect to the horizontal as shown in Fig. 1 related by,

$$\alpha = a\cos\left(\frac{c_0}{c_1}\cos\beta\right), \tag{8}$$

We shall assume that the sound velocity in the bottom is higher than the sound velocity in the water, $c_1 > c_0$, and therefore there exists a critical angle

$$\varphi_{crit} = a\cos\left(\frac{c_0}{c_1}\right) \tag{9}$$

At angles such that $\varphi_0 < \varphi_{crit}$ the incoming wave on the target is an inhomogeneous wave propagating in the horizontal x-direction, with an amplitude decaying exponentially in the vertical z-direction and with particle displacements following elliptical orbits. The scattered wave from the target can be considered as two parts, one part being the normal field and the other part the evanescent field. The normal field occupies the range of real angles $0 < \beta < \pi$ and this field is transmitted back to the angle interval in the water $\varphi_{crit} < \alpha < (\pi - \varphi_{crit})$. The evanescent parts of the scattered field in the bottom correspond to imaginary values of the scattering angle β. These parts are

transmitted back to the intervals $0 < \alpha < \varphi_{crit}$ and $(\pi - \varphi_{crit}) < \alpha < \pi$ in the water. As we want to determine the scattering for all angles $0 < \alpha < \pi$ it follows that it is necessary to determine the scattered wave, when the incoming wave on the target is inhomogeneous. We will discuss this in the next paragraph for the special case of a spherical object.

3

Scattering of a spherical object

The objective of this analysis is to study the scattering of objects at grazing angles lower than critical angle. Therefore we will assume a simple target in order not to be distracted by the more complicated scattering from a more complicated target. We take as an example, the scattering from a completely rigid sphere, but the result can be extended to fluid or solid spheres, spherical shells and with minor modifications, to infinite, long objects with cylindrical symmetry.

For a rigid sphere, the classical paper by Anderson [4], considers the incident wave propagating in the negative x-direction is

$$\phi_i = \phi_1 \, exp\left[i\left(-k_1 x - \omega t\right)\right], \tag{10}$$

with wave number $k_1 = \omega / c_1$. This incident field is expanded in spherical waves by an infinite sum of spherical Bessel functions, $j_m(kr)$ and Legendre polynomials $P_m(cos\theta)$,

$$\phi_i = \phi_1 \sum_{m=0}^{\infty} (-i)^m (2m+1) P_m(\cos\theta) j_m(k_1 r) \exp(-i\omega t). \tag{11}$$

The scattered field is expressed in a similar manner by,

$$\phi_s = \sum_{m=0}^{\infty} A_m P_m(cos\theta)\left[j_m(k_1 r) + i y_m(k_1 r)\right] exp(\left(-i\omega t\right). \tag{12}$$

The unknown coefficients A_m are determined by the boundary condition. For a completely rigid sphere, the boundary condition is that the total particle displacement is zero on the surface of the sphere. The unknown coefficients are then found as

$$A_m = -\phi_0 \left(-i\right)^m \left(2m+1\right) \frac{1}{1 + iC_m}, \tag{13}$$

with

$$C_m = \frac{y_m'(k_0 a)}{j_m'(k_0 a)}. \tag{14}$$

This is the result for a rigid sphere, a fluid or elastic sphere and for a spherical shell the results are given in the literature for instance by Anderson [4], Faran [5], Hickling [6] and Zhen [7].

By applying the asymptotic value of the Bessel functions, the far field scattered wave is found as

$$\phi_s = \frac{i}{k_1 r}\phi_1 \, exp\left(ik_1 r - i\omega t\right)\sum_{m=0}^{\infty}(-1)^m(2m+1)P_m(cos\theta)\frac{1}{1+iC_m}. \tag{15}$$

The result is normalized by the scattering from a perfect scattering sphere $\sigma_s = (a/2)^2$ giving the normalized scattering cross section,

$$\tilde{\sigma}_{bs} = \frac{4}{(k_1 a)^2}\left|\sum_{m=0}^{\infty}(-1)^m(2m+1)\frac{1}{1+iC_m}\right|^2. \tag{16}$$

The normalized scattered amplitude as function of angle at a reference distance of 1 m, is therefore expressed by the scattering function $S(\theta)$

$$S(\theta) = \frac{2}{k_1 a}\left|\sum_{m=0}^{\infty}(-1)^m(2m+1)P_m(cos\theta)\frac{1}{1+iC_m}\right|. \tag{17}$$

The far field assumption requires that $k_1 r >> 1$, an assumption that is satisfied as the minimum distance between the centre of the sphere and the interface is equal to the radius and relatively large spheres are considered.

The expression $S(\theta)$ in Eq. (17) gives the scattering in direction θ with respect to the direction of the incoming wave. For the target in the bottom the incoming wave has the direction φ_1 and the direction of the scattering is β, both angles with respect to the horizontal as shown in Fig. 1. The scattering function to use in Eq. (5) is therefore $S_1(\beta,\varphi_1) = S(\beta - \varphi_1)$. In the case of an incoming wave at angle lower than critical angle, the angle φ_1 is imaginary and β covers a range of both real and imaginary angles corresponding to all real angles α in the interval $(0-\pi)$ for the direction of the scattering back to the water (Eq. (8)). For a sphere it is therefore necessary to calculate Legendre polynomials for imaginary arguments. This is done as for the real cases by applying the normal recursive equations [8].

For the case of angles lower than critical angle, the argument θ in the above equations is imaginary and therefore requires the calculation of the Legendre polynomials for imaginary arguments. This is done as for the real cases by applying the normal recursive equations [8].

Figure 2 shows the normalized backscattering coefficient of Eq. (16) as function of $k_0 a$ and the scatter diagram, Eq. (17), for a rigid sphere with $k_0 a = 5$. As stated above, this result is normalized with respect to the scattering of an ideal sphere with scattering cross-section equal to the geometrical cross section. The normalization is removed by multiplying the scattered amplitude with $a / 2$.

Two bottom types will be considered, referred to as sand and silt, with properties given in Table 1. The water is assumed to have $\rho_0 = 1000\ kg / m^3$ and $c_0 = 1500\ m / s$.

Table 1 *Bottom properties*

Sediment	Density (ρ_1)	Sound velocity (c_1)
Sand	$2000\ kg / m^3$.	$1800\ m / s$.
Silt	$1500\ kg / m^3$.	$1650\ m / s$.

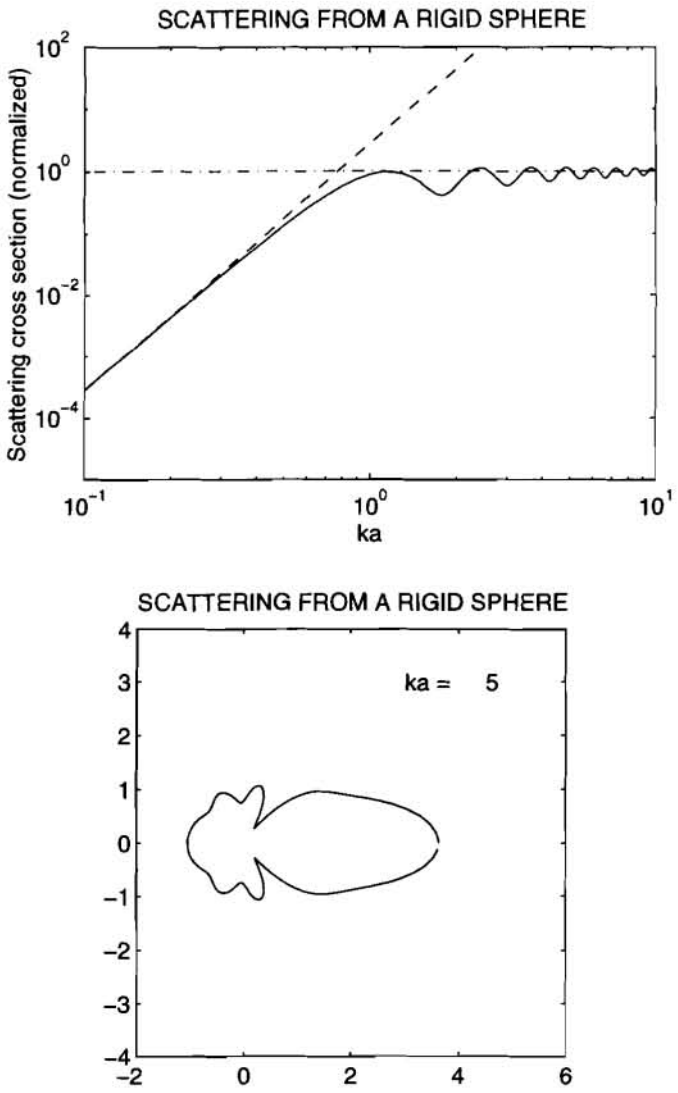

Figure 2 (a) *Backscattering coefficient as function of ka.*
(b) *Directivity of scattering for ka=5.*

To illustrate the effect of an incoming inhomogeneous wave on the target, consider the case of a rigid sphere with the size of $k_0 a = 5$ in water and somewhat lower value in the sediment, due to the higher sound speed.

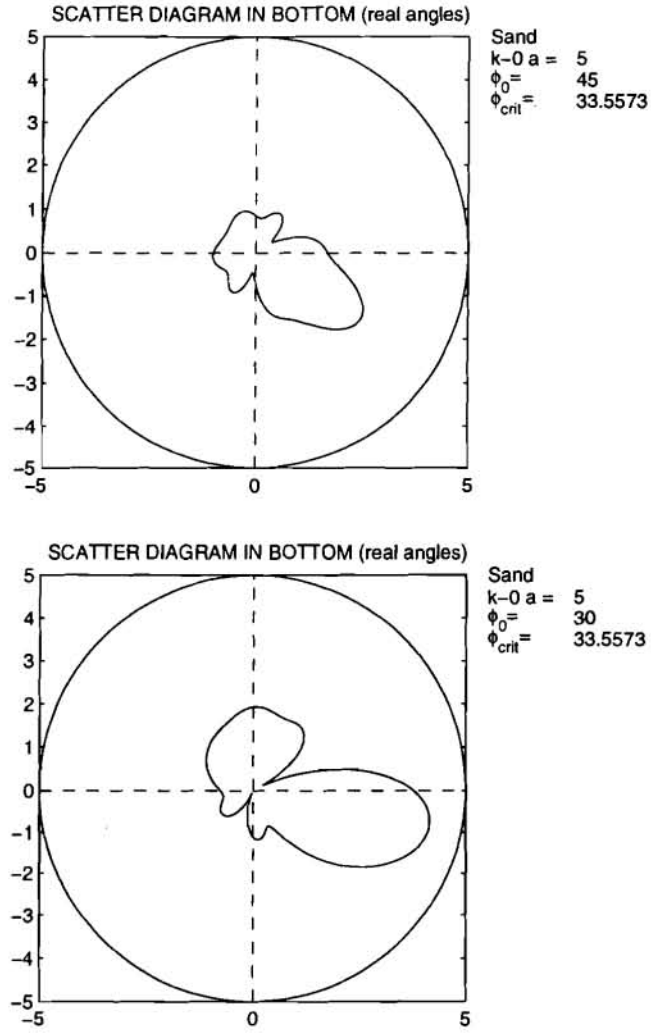

Figure 3 *Scatter diagram in the bottom for an incoming wave with grazing angle* $\varphi_0 = 30^0$. *Sand bottom with target size* $k_0 a = 5$.

Figure 3 shows examples of polar plots of the scattered field in the bottom. In Fig. 3a the incoming wave is at 45° which is higher than the critical angle. Figure 3b is for an incoming wave at 30°, lower than critical. In the latter case, the scatter diagram is completely changed and the shape is no longer symmetric. This is as expected due to the asymmetry of the inhomogeneous wave. From Fig. 3b, it also appears that the amplitude of the scattered field is increased in the inhomogeneous case. This is however not true as the scattered amplitude will be reduced with the decay factor $\exp(-\gamma_z z_t)$ with

$$\gamma_z = k_1 \sin\varphi_1 = \sqrt{k_0^2 \sin\varphi_0 - k_1^2}\ . \tag{18}$$

This factor reduces the amplitude of the scattered wave so that amplitude will be less than for the homogeneous case. The scattered field of the inhomogeneous wave is less reduced than the amplitude decay factor at the depth of the centre of the sphere, as the amplitude of the incoming wave is larger on the top of the sphere than at the centre or at the bottom. The stronger isonification at the top of the sphere is a consequence of the exponential decay resulting in an enhancement of the scattering towards the near-vertical direction.

Figure 4 shows an example of how the scattered field in the bottom is transmitted back into the water. The lower panel shows the amplitude of the upward part of the scattered field in the bottom which is transmitted back into the water to occupy the angle interval $\varphi_{crit} < \alpha < (\pi - \varphi_{crit})$. In addition there is an evanescent field in the bottom corresponding to imaginary values of β which can not be shown in the figure. This field is transmitted back to the intervals $0 < \alpha < \varphi_{crit}$ and $(\pi - \varphi_{crit}) < \alpha < \pi$ and is quite low.

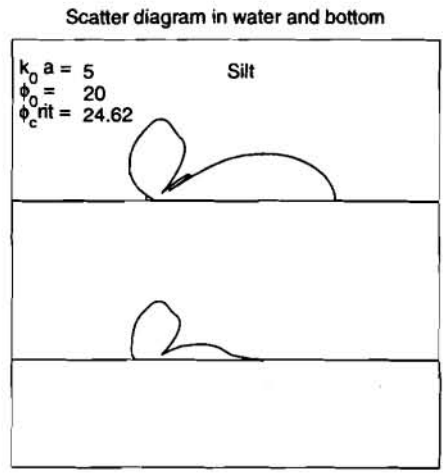

***Figure 4** Transmission of scattering from bottom back into water.*
Lower panel: Scattering function in bottom.
Upper panel scattering function in water.

Figure 5 shows three examples of scattered field as function of scattering angles for a sphere with $k_0 a = 5$. Figure 5a is for the case when the sphere is in water; this case is included as a reference case. The two other figures are for the same sphere at the same location but buried in sand at depth $z_t = a$, which is flush with the water-bottom interface. The angles of the incoming waves are $\varphi_0 = 35^\circ$ and $\varphi_0 = 30^\circ$ respectively for

Figs. 5b and 5c. As the critical angle in this case is $\varphi_{crit} = 33.6^{\circ}$, these angles are slightly above and below the critical angle.

For the sphere in the water, the level of the scattered field oscillates around 0 dB as a consequence of normalization. The deviation from this level is a result of the structure of the scattered field which also can be seen in Fig. 2.

Figure 5b shows that for the buried target and incoming wave above the critical angle, the scattered field has the same amplitude, but the backscattering is confined to angles above the critical angles.

Figure 5c shows the effect when the incoming grazing angle is lower than the critical angle. There is now a scattered field at angles lower than the critical angle, quite low in the backward direction and significantly higher in the forward direction. The maximum scattering is found in a wide angle interval around the vertical direction, but this field is reduced compared with the cases shown in Figs. 5a and 5b.

Figure 6 illustrates the effect of frequency. The target scattering strength is calculated for three values of normalized target size, $k_0 a = 5, 10$ and 20, respectively for Figs. 6a, 6b and 6c. The target is buried in silt at depth $z_T = a$ and the incoming wave in the water has the grazing angle $\varphi_0 = 20^{\circ}$, which is below critical angle. The results are normalized with respect to target size and frequency, but the three cases can be taken as corresponding to a target with radius $a = 0.5m$ for the sonar frequencies of 2.5 kHz, 5kHz and 10 kHz respectively. The figures show that the evanescent backscattered field is strongly affected by frequency and tends to disappear completely for higher frequencies. For the other scattering angles, the echo levels decrease less significantly with frequency and are nearly constant in the near-vertical direction.

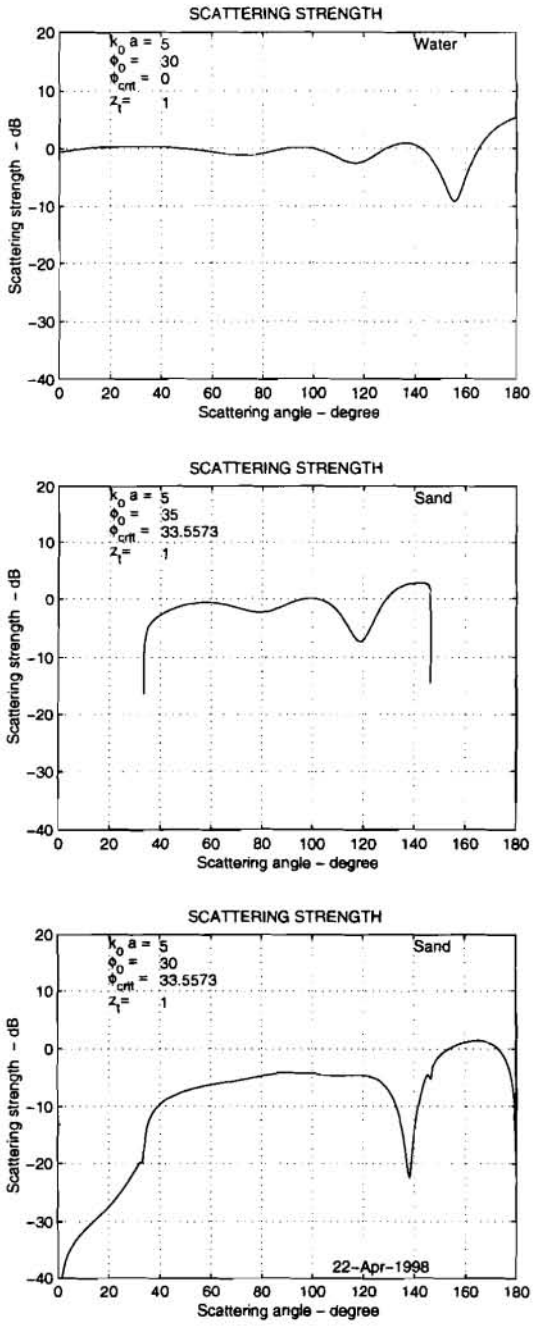

Figure 5 *Scattering from a sphere with*
a) Sphere in the water.
b) Buried sphere in sand, incoming angle above critical.
c) Buried sphere in sand, incoming angle below critical.

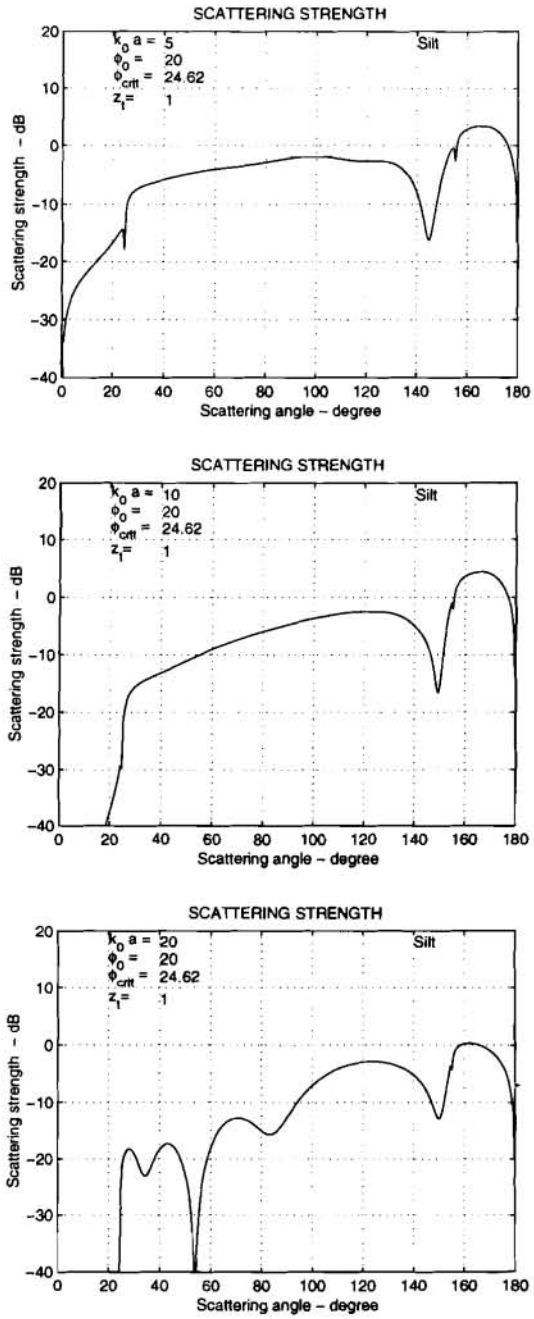

Figure 6 *Effect of frequency, rigid sphere with a=0.5 m.*
a) Frequency 2.5 kHz.
b) Frequency 5.0 kHz.
c) Frequency 10.0 kHz.

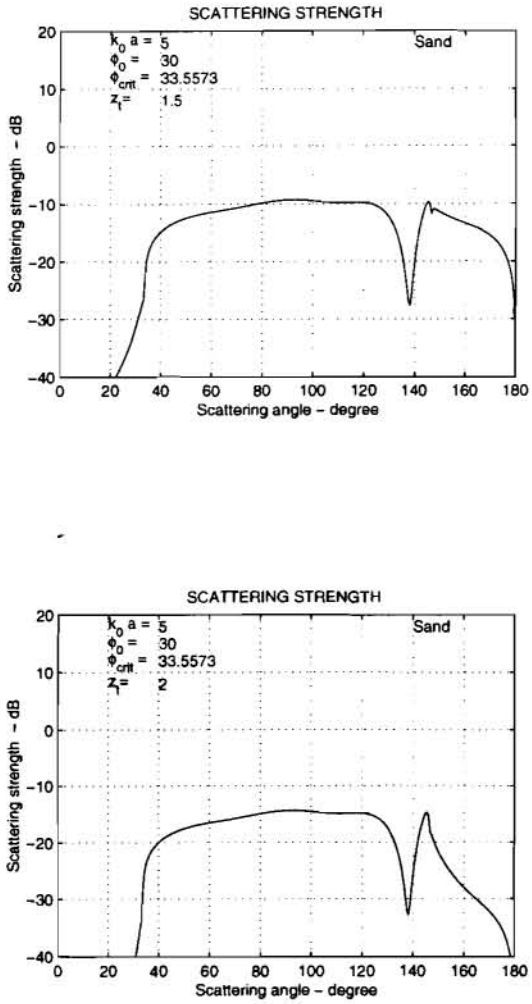

Figure 7 *Effect of depth. Sphere buried in sand at depths*

a) $z_T = 1.5a$

b) $z_T = 2.0a$

Figure 7 shows the effect of depth of burial with $z_T = 1.5a$ and $z_T = 2a$, Fig. 5 c shows the same case with $z_T = a$. The grazing angle of the incident field is $\varphi_0 = 30^\circ$ which is lower than the critical angle for this sand bottom. The echo from a deeper buried target is reduced considerably for angles less than critical, due to the effect of exponential decay.

4

Signal-to-reverberation ratios.

The intention of this section is to give some indication of the signal-to reverberation ratio achievable in detection of a buried object, applying the results of the previous section. In most cases, the detectability of a target on or buried in the bottom is limited by bottom reverberation. As the current interest is focused on monostatic detection at low grazing angles as well as bistatic detection over a wide angle interval, it is not easy to find bottom scattering values and models which are correct for all cases. The scattering model used in this study, is based on the small-roughness approximation perturbation known as the Rayleigh-Rice approximation. This scattering model is used for backscattering and forward scattering by Jackson, Winebrenner and Ishimaru [9] and Essen [10], [11]. The model is simple but has limitations at high grazing angles and at angles close to the specular direction, but is generally assumed to be reasonably correct for small grazing angles. In future studies of detection of buried objects, bottom reverberation needs to be considered much more rigorously.

According to this model, the scattering strength in the direction φ_s as resulting from an incoming plane wave at direction φ_s is given as,

$$\sigma_s(\varphi_s,\varphi_0) = 4k_0^4 \sin^2\varphi_s \sin^2\varphi_0 T(\varphi_s,\varphi_s,\nu,\rho) W(k_0\cos\varphi_0 + k_0\cos\varphi_s), \tag{19}$$

where $T(\varphi_s,\varphi_s,\nu,\rho)$ is a function which, in addition to the two angles, depends on the relative density $\rho = \rho_1 / \rho_0$ and the relative sound speed $\nu = c_1 / c_0$. The expression can be found in Essen [11]. The spectrum of the roughness has the form $W(k)$ it is important to choose the appropriate function for this spectrum. Following Essen, it is assumed that $W(k)$ follows a power law of the form

$$W(k) = \begin{cases} \dfrac{G_0}{2\pi} k^{-\gamma} & \text{for} \quad k > k_u \\ 0 & \text{for} \quad k < k_u \end{cases}. \tag{20}$$

Comparison with experimental values often suggests that an appropriate value for the exponent is $\gamma \approx 3.5$. However, the value of $\gamma = 4$ is especially attractive in a study of this kind, as it renders the backscattering independent of frequency, as can be seen from Eq. (19). With this spectrum the scattering strength for low angles is proportional $\tan^2(\varphi_0)\tan^2(\varphi_s)$

The cutoff wavenumber k_u is necessary to prevent the singularity which otherwise occurs at $k = 0$. This singularity appears at the specular direction in forward scattering when $\phi_s = \pi - \varphi_0$ and at normal incidence in the backscattering situation where $\phi_s = \varphi_0$. The cutoff wavenumber truncates the scattering for angles given by,

$$\left| k_0 \cos\varphi_0 + k_0 \cos\varphi_s \geq k_u \right| . \tag{21}$$

This value may also be considered as defining the limit of validity. As an example, with $\varphi_0 = 15^\circ$ and $k_u = 20 m^{-1}$ Eq. (20) requires that $\varphi_s < 120^\circ$ for a frequency of 10 kHz, $\varphi_s < 90^\circ$ for a frequency of 5 kHz and $\varphi_s < 20^\circ$ for a frequency of 2.5 kHz. As the value of k_u does not affect the shape of the scattering function but only the validity, we have chosen to plot the backscattering as if $k_u = 0$ with the caveat that the limits given above should be remembered when discussing the signal - to -reverberations ratios in the next section.

The accuracy of the perturbation method and the alternative Gaussian roughness spectrum is treated by Thorsos and Jackson [12] This spectrum may be a better choice for large scattering angles, but for backscattering and bistatic scattering at low angles, the chosen power law spectrum is preferable.

The value of G_0 is chosen to give a best fit to measured values. According to Jackson *et al* [9] the value $G_0 / 2\pi = 0.004$ gives the best fit to measured date, at least for the backscattering direction.

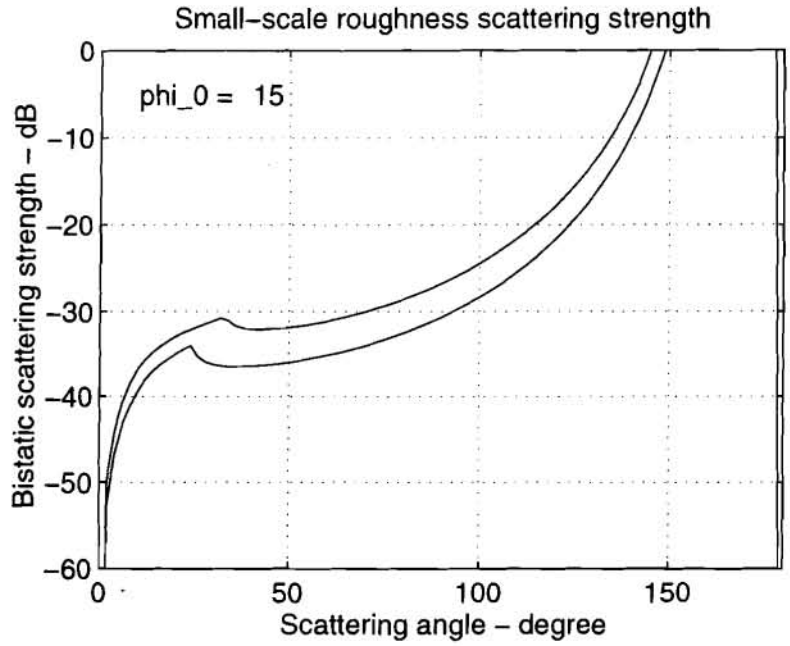

Figure 8 *Bottom scattering strength as function of scattering grazing angle for an incoming wave at* $\varphi_0 = 15^\circ$.

Figure 8 shows examples of backscattering strength as function of the scattering angle φ_s for an incoming wave with grazing angle $\varphi_0 = 15^\circ$ for the bottom types specified in Table 1. There is a sharp increase when approaching the specular direction of 165° which is in contradiction to observations and illustrates the limitation of this model and spectrum as discussed earlier.

The bottom reverberation level at the receiver at distance r is

$$I_B(r) = I_0 \frac{A}{r^2} \sigma_s(\varphi_s, \varphi_0) \tag{22}$$

where the incident intensity is I_0, A is the sonar patch size and $\sigma_s(\varphi_s, \varphi_0)$ is given by equation18.

The normalized echo level is

$$I_E(r) = I_0 \frac{1}{r^2} S^2{}_0(\varphi_s, \varphi_0) \tag{23}$$

where $S_0(\varphi_s, \varphi_0)$ is the scattered field of the object found by the procedure described in the previous section.

The sonar patch size A is given by the beamwidth of the sonar, the effective compressed pulse length and the geometry of the situation. As this is not known, the examples assume that the patch size is a given number, N_A, larger than the geometrical cross section of the target

$$A = N_A\left(\pi a^2\right) \tag{24}$$

Normalizing the bottom reverberation level with respect to the echo level from an ideal sphere, means that the normalized patch size is

$$A_{norm} = 4\pi N_A \tag{25}$$

In the following examples the patch size number is always $N_A = 10$. The effect of a larger or smaller patch size is easy to account for as the reverberation level increases with $10\log(A)$.

Figures 9 and 10 show examples of computed signal and reverberation levels for the two media 'sand' and 'silt' (Table 1). The examples are chosen to illustrate what may happen when transmitting close to the critical angle. The figures show the estimated signal and reverberation levels as function of scattering angle for a given incident grazing angle. The monostatic levels are found by reading the levels for the scattering angle, equal to the incident grazing angle. The levels are normalized with respect to the echo of an ideal sphere, with scattering section equal to the geometrical cross-section, located on the same position and in water.

In all cases there appears to be a broad angle interval from about to 40° to 120° where the scattered signal from the target is maximum. The maximum signal - to- reverberation ratio is found in an interval from above the critical angle to about 90°. This interval may extend to greater angles as the reverberation model may overestimate the reverberation level for higher angles.

When transmitting at angles below critical angle, (Figs. 9a-b, and 10a-b), there are evanescent field contributions at angles closer to the horizontal than the critical angle, in backward and forward directions The backward scattered field is quite weak compared with the scattered field above the critical angle.

When the transmission is at angles above the critical angle, the scattering of the target is limited to angles above the critical angle. The effect of the burial is then a relatively minor reduction of amplitude due to transmission loss at the interface.

The figures show that an object buried in silt is a better target than an object buried in sand. This result is partly a consequence of the reverberation model and partly because of a slightly higher echo level for a target buried in silt than in sand.

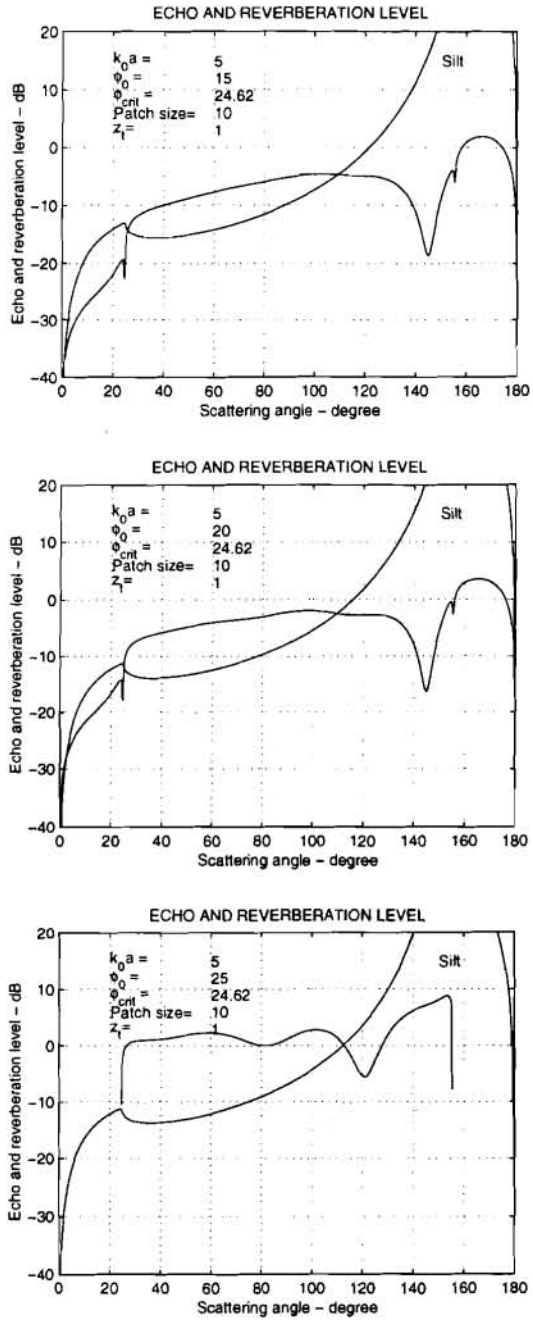

Figure 9 *Signal and reverberation for a target buried in silt.*
For grazing angle of the incoming wave $\varphi_0 = 15^\circ$, $\varphi_0 = 20^\circ$ *and* $\varphi_0 = 25^\circ$.
Critical angle $\varphi_{crit} = 24.6^\circ$.

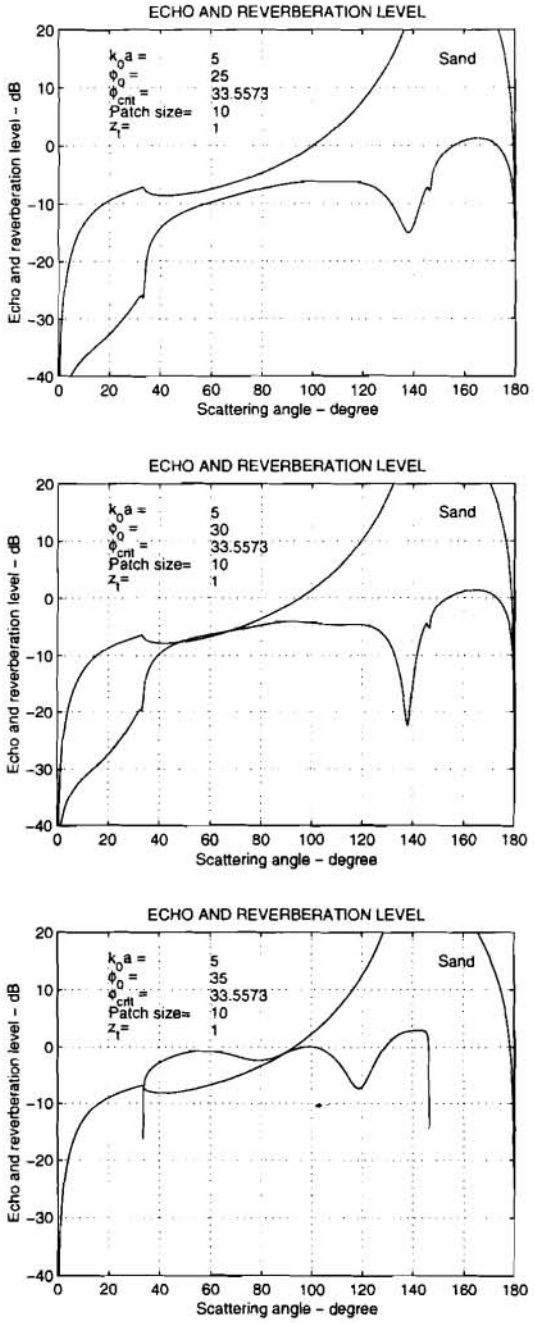

Figure 10 *Signal and reverberation for a target buried in sand.*
For grazing angle of the incoming wave $\varphi_0 = 25^\circ$, $\varphi_0 = 30^\circ$ *and* $\varphi_0 = 35^\circ$.
Critical angle $\varphi_{crit} = 33.6^\circ$.

5 Conclusions

The scattering from a rigid sphere buried in the bottom has been determined for all grazing angles. For angles lower than critical, the wave impacting on the target is inhomogeneous and the scattered field is strongly modified in angular distribution. For angles higher than critical the scattered amplitude for a shallow buried target is only moderately reduced, compared with scattering of a proud sphere.

In a detection situation, bottom reverberation is expected to be the limitation. The signal and reverberation levels are estimated for the case of the buried rigid sphere. The bottom reverberation is calculated using the small-roughness perturbation approximation, with a surface roughness spectrum which makes the scattering level independent of frequency.

Several examples are presented with the target buried in sand and silt. Emphasis is on situations with a transmitted signal close to critical angle, for monostatic and bistatic detection situations.

These conclusions derive from a very simple model. For more realistic situations, the conclusions and observations given above are valid but there may be other factors which are important. It is however quite feasible to extend this analysis to the case of a solid bottom with shear wave conversion at the interface and at the target. It may also be possible to consider at porous fluid or solid bottom and to include the effect of the Biot second wave.

Acknowledgment.

The fruitful discussion and comments by John Fawcett, Henrik Schmidt and Marc Pinto are deeply appreciated

References

[1] Lim, R., Lopes, J., L., Hackman, R.,H., and Todoroff, D.G. Scattering by objects buried in underwater sediments: Theory and experiments. *Journal of the Acoustical Society of America*, **93**, 1993:1762-1782,.

[2] Tamsauskas, H.,T., Fawcett, J.A. Scattering by spheres buried in sediment. SACLANTCEN SM-324. La Spezia, Italy, 1997.

[3] Ingenito, F. Scattering from an object in a stratified medium. *Journal of the Acoustical Society of America*, **82,** 1987:2051-2069.

[4] Anderson, V.C. Sound scattering from a fluid sphere. *Journal of the Acoustical Society of America*, **22,** 1950:426-431.

[5] Faran, J.J. Sound scattering by solid cylinders and spheres, *Journal of the Acoustical Society of America*, **23,** 1951:405-418.

[6] Hickling, R. Analysis of echoes from a solid elastic sphere in water, *Journal of the Acoustical Society of America*, **34,** 1962:1582-1592.

[7] Zhen Ye. On sound scattering and attenuation of Albunex ® bubbles. *Journal of the Acoustical Society of America*, **100,** 1996:2011-2028.

[8] Morse, P.M., Ingard, K.U. Theoretical Acoustics. New York, McGraw Hill Inc., 1968.

[9] Jackson, D.R., Winebrenner, D.P., Ishimaru, A. Application of the composite scattering model to high-frequency bottom backscattering. *Journal of the Acoustical Society of America*, **79,** 1986:1410-1422.

[10] Essen, H.-H. Scattering from sedimental seafloor containing shear and layering, *Journal of the Acoustical Society of America* **95** (3), 1299-1310, 1994.

[11] Essen, H.-H. Perturbation theory applied to sound scattering from a rough sea-floor. SACLANTCEN SR-194, La Spezia, Italy, 1992.

[12] Thorsos E.I., Jackson, D.R. The validity of the perturbation approximation for rough surface scattering using a Gaussian roughness spectrum. *Journal of the Acoustical Society of America*, **88**, 1990:261-277.

Report no. changed (Mar 2006): SR-279-UU

Document Data Sheet

Security Classification		Project No.
UNCLASSIFIED		031-1
Document Serial No.	Date of Issue	Total Pages
SR-279	October 1998	28 pp.

Author(s)

Hovem, J.M.

Title

Detection of buried objects in the seabed - a simple model study

Abstract

The problem of detecting an object buried in the seabed is studied by means of a simple model. In this model, the object is a rigid sphere buried in a bottom modelled as a fluid half space. The scattered field is determined for all angles, including grazing angles lower than the critical angle. The analysis shows that the scattered field is considerably changed in amplitude and angular distribution, when the incoming wave is an inhomogeneous wave. There is relatively strong scattering in a broad angle interval, near the vertical direction. The detectability of a buried target is determined by the echo-to-reverberation level. This issue is discussed using a simple bottom reverberation model based on the small-roughness perturbation approximation. Signal-to-reverberation ratios are computed for different bottom types and for angles lower and higher than critical angle, for monostatic and bistatic detection situations.

Keywords

Issuing Organization

North Atlantic Treaty Organization
SACLANT Undersea Research Centre
Viale San Bartolomeo 400, 19138 La Spezia,
Italy

*[From N. America: SACLANTCEN
(New York) APO AE 09613]*

Tel: +39 0187 527 361
Fax:+39 0187 524 600

E-mail: library@saclantc.nato.int

Initial Distribution for SR 279

Ministries of Defence

DND Canada	10
CHOD Denmark	8
DGA France	8
MOD Germany	15
HNDGS Greece	12
MARISTAT Italy	9
MOD (Navy) Netherlands	12
NDRE Norway	10
MOD Portugal	5
MDN Spain	2
TDKK and DNHO Turkey	5
MOD UK	20
ONR USA	34

NATO Commands and Agencies

NAMILCOM	2
SACLANT	3
CINCEASTLANT/ COMNAVNORTHWEST	1
CINCIBERLANT	1
CINCWESTLANT	1
COMASWSTRIKFOR	1
COMMAIREASTLANT	1
COMSTRIKFLTANT	1
COMSUBACLANT	1
SACLANTREPEUR	1
SACEUR	2
CINCNORTHWEST	1
CINCSOUTH	1
COMEDCENT	1
COMMARAIRMED	1
COMNAVSOUTH	1
COMSTRIKFORSOUTH	1
COMSUBMED	1
NC3A	1
PAT	1

Scientific Committee of National Representatives

SCNR Belgium	1
SCNR Canada	1
SCNR Denmark	1
SCNR Germany	1
SCNR Greece	1
SCNR Italy	1
SCNR Netherlands	2
SCNR Norway	1
SCNR Portugal	1
SCNR Spain	1
SCNR Turkey	1
SCNR UK	1
SCNR USA	2
French Delegate	1
SECGEN Rep. SCNR	1
NAMILCOM Rep. SCNR	1

National Liaison Officers

NLO Canada	1
NLO Denmark	1
NLO Germany	1
NLO Italy	1
NLO Netherlands	1
NLO Spain	1
NLO UK	1
NLO USA	1

Sub-total	200
SACLANTCEN	30
Total	230